Multiphoton ionization and stabilization of helium in superintense xuv fields

S. A. Sørngård, S. Askeland, R. Nepstad, and M. Førre
Department of Physics and Technology, University of Bergen, N-5007 Bergen, Norway
(Received 19 January 2011; published 21 March 2011)

Multiphoton ionization of helium is investigated in the superintense field regime, with particular emphasis on the role of the electron-electron interaction in the ionization and stabilization dynamics. To accomplish this, we solve *ab initio* the time-dependent Schrödinger equation with the full electron-electron interaction included. By comparing the ionization yields obtained from the full calculations with the corresponding results of an independent-electron model, we come to the somewhat counterintuitive conclusion that the single-particle picture breaks down at superstrong field strengths. We explain this finding from the perspective of the so-called Kramers-Henneberger frame, the reference frame of a free (classical) electron moving in the field. The breakdown is tied to the fact that *shake-up* and *shake-off* processes cannot be properly accounted for in commonly used independent-electron models. In addition, we see evidence of a change from the multiphoton to the shake-off ionization regime in the energy distributions of the electrons. From the angular distribution, it is apparent that the correlation is an important factor even in this regime.

DOI: 10.1103/PhysRevA.83.033414 PACS number(s): 32.80.Fb, 32.80.Rm

I. INTRODUCTION

More than 20 years ago, theoretical studies of atomic hydrogen in ultraintense, high-frequency laser fields produced an unexpected result [1–9]: When increasing the intensity of the laser pulse to such a degree that the applied forces dominate over the Coulomb attraction between the nucleus and the electron, the ionization probability does not increase accordingly but rather stabilizes or starts subsiding. This counterintuitive phenomenon was dubbed atomic stabilization and was subject to much research in the following decade. The discussions, controversies, and conclusions are available in a number of review articles. (See, e.g., [10–12] and references therein.) It has also been pointed out that atomic stabilization has a classical counterpart [13,14]. (See also [10] and references therein.)

At the start of the 1990s, the laser technology required to experimentally observe the stabilization effect in tightly bound systems was not available. For example, in order to measure the stabilization in atomic hydrogen, photon energies exceeding 13.6 eV, the binding energy of the atom, and intensities on the order of 10^{16} W/cm^2 or more are required [15,16]. Grobe and Eberly [17] demonstrated that stabilization could occur in H^- at moderate intensities ($\sim 10^{13}$ W/cm^2) and photon energies ($\sim$2 eV), and Wei *et al.* [18] suggested an experiment in which a laser, of realistic frequency and intensity, could possibly stabilize the unstable He^- ion. However, at present, the only experimental confirmations of stabilization are from studies of low-lying Rydberg states [19–22]. With recent advances in free-electron laser (FEL) technology, extremely high peak intensities have been achieved, with wavelengths ranging from vacuum ultraviolet to soft x rays [23,24], and even higher intensities are expected to be delivered in the near future [25]. Thus, laser technology is approaching the regime needed for observing atomic stabilization in ground-state (neutral) atomic systems.

Although atomic stabilization has been studied extensively during the last two decades, studies of stabilization in systems containing two electrons are still scarce [10,26], and most often assessed with simplified physical models of reduced dimensionality. A study on stabilization in a model two-electron xenon atom revealed that both the single- and double-ionization channels may be subjected to stabilization [27,28]. However, it has also been pointed out that the electron-electron interaction suppresses atomic stabilization [17,29–31]. Including a second electron adds a new dimension to the problem, manifested through the electronic repulsion. Although *ab initio* calculations of helium have previously been performed at fairly high intensities in the extreme ultraviolet (xuv) regime [32,33], only recently were such endeavors extended into the stabilization regime [34], confirming the detrimental effect of the electron-electron interaction on stabilization. However, it was shown that the effect is markedly less than predicted in models of reduced dimensionality.

In this paper, we revisit the problem of the multiphoton ionization of helium in superintense, high-frequency fields. In continuation of the work of Birkeland *et al.* [34], we look more closely into the strong-field-ionization dynamics of the atom, with particular emphasis on atomic stabilization, considering laser pulses of various central frequencies and durations. A comparison of the ionization yields obtained from the *ab initio* calculations, including correlations, with corresponding results obtained from an independent-electron model reveals that the validity of the latter breaks down at strong fields. An analysis of the system equations in the so-called Kramers-Henneberger frame [35–38] shows that the electron-electron interaction plays a decisive role in this limit. We further show that this is manifested in the energy and angular distributions of the ejected electrons.

Atomic units, where m_e, $\hbar$, and e are scaled to unity, are used throughout unless stated otherwise.

II. METHODS

A. *Ab initio* calculations

We obtain the ionization probability of ground-state helium in extreme laser fields from first principles, i.e., by solving (numerically) the full time-dependent Schrödinger equation (TDSE). Formulating the problem in the velocity gauge, the

Hamiltonian assumes the form

$$H = \sum_{i=1}^{2} \left(\frac{\mathbf{p}_i^2}{2} - \frac{2}{r_i} + A_z(t) p_{z_i} \right) + \frac{1}{|\mathbf{r}_1 - \mathbf{r}_2|}. \quad (1)$$

A sine-squared carrier envelope was chosen for the laser interaction:

$$A_z(t) = A_0 \sin^2\left(\frac{\pi t}{T}\right) \cos(\omega t), \quad (2)$$

where $A_0 = E_0/\omega$, E_0 is the peak amplitude of the electric field, ω is the laser frequency, and T is the total pulse duration. The semiclassical treatment of the field is a valid approach due to the enormous photon flux of superintense lasers.

The pulse fulfills the constraint of a physical pulse [39]:

$$\int_0^T \mathbf{E}(t) dt = 0. \quad (3)$$

Propagation and analysis of the wave function is performed with the PYPROP framework [40], a PYTHON/C++ software package for solving the TDSE.

The wave function is expanded in a B-spline basis [41,42] for each of the radial components, and a coupled spherical harmonic basis for the angular components,

$$\Psi(\mathbf{r}_1, \mathbf{r}_2, t) = \sum_{i,j,k} c_{ijk} \frac{B_i(r_1)}{r_1} \frac{B_j(r_2)}{r_2} \mathscr{Y}_{l_1,l_2}^{LM}(\Omega_1, \Omega_2), \quad (4)$$

where $k = \{L, M, l_1, l_2\}$ is a combined index for the angular indices. The coupled spherical harmonic basis functions

$$\mathscr{Y}_{l_1,l_2}^{LM}(\Omega_1, \Omega_2) = \sum_m \langle l_1 l_2 m M - m | L M \rangle Y_{l_1}^m(\Omega_1) Y_{l_2}^{M-m}(\Omega_2) \quad (5)$$

are obtained by linearly combining products of ordinary spherical harmonics, weighted by Clebsch-Gordan coefficients [43].

As the B-spline basis functions are not orthogonal, an overlap matrix $S_{ij} = \int B_i(r) B_j(r) dr$ is introduced for each electronic coordinate. From these the total overlap matrix is found for every angular momentum component by taking the Kronecker product $\mathbf{S} = \mathbf{I}_k \otimes \mathbf{S}_1 \otimes \mathbf{S}_2$, where $\mathbf{I}_k$ denotes the identity matrix and k is the angular index. The resulting TDSE may then be written as

$$i\mathbf{S} \frac{\partial}{\partial t} \mathbf{c}(t) = \mathbf{H}(t) \mathbf{c}(t) \quad (6)$$

in matrix form.

We solve the TDSE using a scheme based on the first-order approximation to the matrix exponential

$$\exp(-i \Delta t \mathbf{S}^{-1} \mathbf{H}) = \mathbf{I} - i \Delta t \mathbf{S}^{-1} \mathbf{H} + O(\Delta t^2). \quad (7)$$

A direct application of this formula is not desirable due to numerical instabilities. Instead, we combine one half step forward in time

$$\mathbf{c}(t + \Delta t/2) = \left(\mathbf{I} - \frac{i \Delta t}{2} \mathbf{S}^{-1} \mathbf{H} \right) \mathbf{c}(t), \quad (8)$$

with one half step backward in time

$$\mathbf{c}(t + \Delta t/2) = \left(\mathbf{I} + \frac{i \Delta t}{2} \mathbf{S}^{-1} \mathbf{H} \right) \mathbf{c}(t + \Delta t), \quad (9)$$

to obtain the unconditionally stable Cayley-Hamilton form of the time propagator

$$\left(\mathbf{S} + \frac{i \Delta t}{2} \mathbf{H} \right) \mathbf{c}(t + \Delta t) = \left(\mathbf{S} - \frac{i \Delta t}{2} \mathbf{H} \right) \mathbf{c}(t). \quad (10)$$

This linear system of equations is too large to be solved directly; hence, we use an iterative method. Since the matrix $(\mathbf{S} + \frac{i\Delta t}{2} \mathbf{H})$ is not Hermitian, our choice is the generalized minimum-residual method (GMRES), a Krylov subspace method which combines Arnoldi iterations with a least-squares problem in the projected space [44,45]. In the GMRES algorithm, the error in the least-squares residuals is controlled by the dimension of the Krylov subspace, which can be increased until the desired precision is obtained.

B. Calculating ionization

In this paper, we compute the ionization probability resolved in direction and energy. We also do a series of smaller simulations, calculating only the total-ionization probabilities. Separating the single and double ionization is achieved by a projection onto double continuum states. In order to obtain these continuum states exactly, one needs to solve a scattering problem for the full two-particle system. As this is computationally cumbersome, an approximation using single-particle states is adopted instead. It can be described as follows: In the case of double ionization, when both electrons are far from the nucleus, a product of continuum He^+ ($Z = 2$) states is used. For single ionization, when one electron is close to the nucleus and the other far away, a product of bound He^+ and continuum H ($Z = 1$) is used [46].

The single-electron states are not orthogonal to the bound states of the two-electron system, which may become populated during the action of the pulse. Therefore, the projection of the final wave function on the doubly bound states is removed before further analysis is conducted. Moreover, as the electron-electron correlation is neglected in the double continuum states, the system must be propagated after the pulse for all quantities to converge [47].

On the other hand, when only calculating the total ionization, a small radial box is sufficient. It is no longer necessary to propagate the system after the pulse, in order to minimize the interaction term, nor to project onto continuum He^+ states. An absorbing potential is applied at the box boundary in order to absorb the emitted electrons and to minimize reflection. When coupled with an absorbing potential, we find that only about one-third of the radius needed to resolve the differential probabilities is necessary. The total-ionization probability is simply the complement of the probability of being in one of the bound states.

To find the bound states, we use the implicitly restarted Arnoldi method [48]. This is a version of the Arnoldi method for finding eigenpairs that refines the Krylov subspace basis in order to find the wanted eigenvectors and eigenvalues. As the Arnoldi method tends to find the largest eigenvalues, we also use shifted inverse iterations, which let us find the eigenvalues near a given value.

Further details on the discretization, the time integration, and the analysis were presented in a recent paper [49].

C. Independent-electron model

In order to gauge the importance of the electron-electron interaction, we repeat the calculations using an independent-electron (IE) model [50]. The total wave function is approximated as a product of two single-electron wave functions

$$\Psi(\mathbf{r}_1,\mathbf{r}_2) = \psi_{\mathrm{SAE}}(\mathbf{r}_1)\psi_{\mathrm{He}^+}(\mathbf{r}_2). \tag{11}$$

The subscript SAE refers to the single-active electron approximation. This is a common approximation for many-electron problems, which focuses on one electron at a time. Any dependence on the rest of the electrons is included in a common potential that is constant with regard to the other electron positions. To find the first electron wave function ψ_{SAE}, we apply a pseudo potential, which includes the shielding of the nucleus caused by the other electron [51],

$$V(r) = -\frac{Z + a_1 e^{-a_2 r} + a_3 r e^{-a_4 r} + a_5 e^{-a_6 r}}{r}. \tag{12}$$

For helium, the effective charge $Z = 1$ and the coefficients $a_1 = 1.231, a_2 = 0.662, a_3 = 1.325, a_4 = 1.236, a_5 = 0.231$, and $a_6 = 0.480$ were adopted. The other electron moves in a He^+ potential, and it is therefore an accurate model for the singly ionized atom. The IE model reproduces the correct ground-state energies and single- and double-ionization thresholds, and decently represents the excited states. As the name of the model suggests, the electrons do not interact with each other, beyond what is included in the shielded nuclear potential. That makes this a three-dimensional, rather than a six-dimensional problem, and it can be calculated with relative ease on an ordinary computer. As a consequence of working with independent particles, the total- (single + double) ionization probability becomes

$$P^{\mathrm{ion}}_{\mathrm{total}} = 1 - P^{\mathrm{b}}_{\mathrm{SAE}} P^{\mathrm{b}}_{\mathrm{He}^+}, \tag{13}$$

where $P^{\mathrm{b}}_{\mathrm{SAE}}$ and $P^{\mathrm{b}}_{\mathrm{He}^+}$ are the probability of the SAE and the He^+ electron, respectively, being in a bound state. The probability for double ionization is obtained from the product

$$P^{\mathrm{ion}}_{\mathrm{double}} = P^{\mathrm{ion}}_{\mathrm{SAE}} P^{\mathrm{ion}}_{\mathrm{He}^+}, \tag{14}$$

and the single-ionization probability is

$$P^{\mathrm{ion}}_{\mathrm{single}} = P^{\mathrm{b}}_{\mathrm{SAE}} P^{\mathrm{ion}}_{\mathrm{He}^+} + P^{\mathrm{ion}}_{\mathrm{SAE}} P^{\mathrm{b}}_{\mathrm{He}^+}, \tag{15}$$

where $P^{\mathrm{ion}}_{\mathrm{SAE}}$ and $P^{\mathrm{ion}}_{\mathrm{He}^+}$ are the ionization probabilities of the SAE and the He^+ electrons.

D. Convergence of the calculations

When doing the largest calculations, the radial domain typically extends to 80 a.u., although the double of this was employed to test the convergence. A fifth-order B-spline basis of 185 splines is used, distributed exponentially near the nucleus, and linearly further away. Up to 300 splines were used for convergence test purposes. Regarding the angular basis of coupled spherical harmonics, $l \leqslant 5$ and $L \leqslant 6$ were found to be sufficient. Note that the system retains cylindrical symmetry in the presence of the z polarized laser field. Therefore, the M quantum number is set to 0 throughout. Based on the calculations with a larger basis, the error is estimated to be less than 1% in the ionization probabilities.

For the smaller calculations, intended to provide only the total-ionization probability, we use a small radial box of 30 a.u. and 80–100 B splines of order 7, distributed linearly. Note that we have only one-third of the box size but one-half of the number of B splines. In these calculations, the angular basis went up to $l = 7$ and $L = 6$. The small box made it possible to go to higher intensities and pulse lengths than did the large box. The error in the ionization probability is gauged to be less than 5% when $E_0/\omega^2 > 1$ a.u. and less than 2% for lower intensities.

III. RESULTS

A. Ionization probabilities

Figure 1 shows the total- (single + double) ionization probability versus α_0 for three different laser frequencies, $\omega = 4$ (left panel), 5 (middle panel), and 10 a.u. (right panel), and for four different pulse durations, 3, 6, 12, and 24 cycles (from bottom to top). Notice that on the abscissas, the domains are given in $\alpha_0 = E_0/\omega^2$, instead of intensity or peak electric field strength. Here, α_0 represents the displacement amplitude of a free classical electron in the oscillating field [4]. This scaling allows us to easily compare the results obtained with different laser frequencies. In most of the considered cases, the ionization probability increases with α_0 up to some point, where it attains a maximum before it starts to decline, i.e., we are entering the so-called stabilization regime. When stabilization occurs, the ionization peak (corresponding to the "death valley" [10]) is typically situated between $\alpha_0 = 0.6$ and

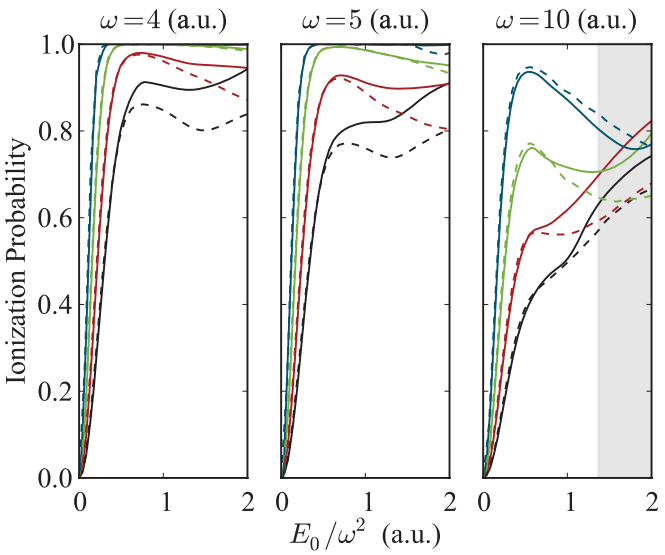

FIG. 1. (Color online) Ionization probabilities plotted as functions of the electronic displacement (E_0/ω^2) for the frequencies $\omega = 4$ (left panel), $\omega = 5$ (middle panel), and $\omega = 10$ a.u. (right panel). In each panel, the pulses are of 3, 6, 12, and 24 cycles duration from bottom to top. The solid lines are the results from the full calculations. The dashed lines are the results from the IE calculations. In the right panel, the displacement (α_0) extends into a region (shaded) where relativistic (nondipole) effects may have an influence on the results [15,30,31,52], and the corresponding velocity of a classical free electron moving in the field exceeds 10% of the speed of light.

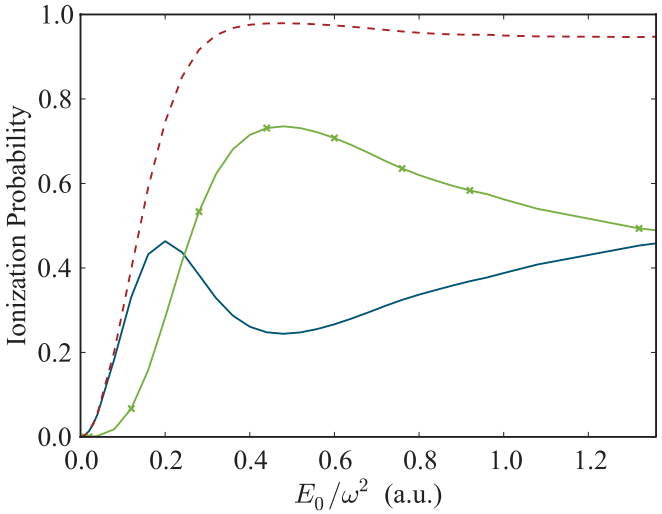

FIG. 2. (Color online) Single (full blue line), double (full green line with crosses) and total (dashed red line) ionization probabilities plotted against the electronic displacement for the case of a 6-cycle pulse with $\omega = 4$ a.u.

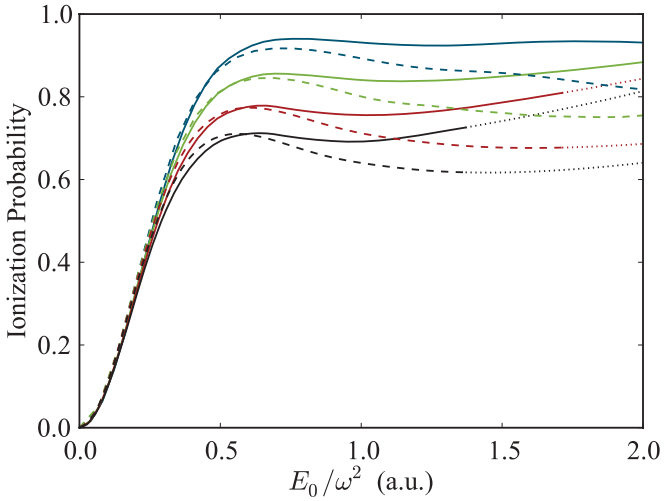

FIG. 3. (Color online) Ionization probabilities for a constant pulse duration of 2π a.u. The lines correspond to laser frequencies of $\omega =$ 4, 6, 8, and 10 a.u. from top to bottom, or equivalently pulse lengths of 4, 6, 8, and 10 cycles. The solid lines are the full calculations. The dashed lines are the IE calculations. The dotted parts of the curves indicate where relativistic (nondipole) effects may influence the results.

0.7 a.u., independent of laser frequency and pulse duration. For very short pulse durations, e.g., the three-cycle pulse of $\omega = 10$ a.u., we observe a knee in the function, rather than a peak at the stabilization point. This is probably due to the relatively large bandwidth of these short pulses and the averaging this leads to. For long pulse durations, e.g., the 24-cycle pulse of $\omega = 4$ a.u., the atom is almost fully ionized, and the stabilizing effect turns out to be weak. The dashed lines in the figure are the results of the independent-electron model. They show good agreement with the full calculations for weak fields ($\alpha_0 < 0.5$ a.u.) and for long pulses, but otherwise tend to overestimate the stabilization. As a matter of fact, the results show that the electron-electron interaction suppresses stabilization in all cases. We will return to the reason for this later.

In Fig. 2, we examine in more detail the case with 6 cycles and $\omega = 4$ a.u., showing both the total-ionization probability and its single- and double-ionization components. Both the single- and double-ionization probabilities peak at specific values of the field, which is in qualitative agreement with the results of Volkova *et al.* [27] and Popov *et al.* [28]. As expected, the single ionization dominates for weak fields, but it peaks at $\alpha_0 \simeq 0.2$ a.u., where the probability for double ionization starts to increase rapidly. From $\alpha_0 \simeq 0.3$ a.u. on, double ionization is the dominant ionization channel. Then, the double-ionization probability attains a maximum value at the point where the single-ionization probability reaches its minimum, i.e., at $\alpha_0 \simeq 0.5$ a.u. The subsequent decrease in the double-ionization probability, in the stabilization regime, is accompanied by a corresponding rise in the single-ionization yield. This feature is a characteristic of the stabilization dynamics of helium in few-cycle laser pulses [34].

Figure 3 shows the ionization probability as a function of α_0 for a pulse of constant duration $T = 2\pi$ a.u., but for varying frequencies, $\omega = 4$, 6, 8, and 10 a.u. The corresponding results of the IE model are shown in dashed lines. One immediately perceives that for higher frequencies, the atom stabilizes at lower ionization probabilities, in accordance with the results in Fig. 1. Note that in the limit of weak fields, single ionization is by far the dominating ionization channel. Thus, from first-order perturbation theory, $P_{\text{total}}^{\text{ion}} \propto \alpha_0^2 T$. Now, since the pulse duration is kept fixed in Fig. 3 (as opposed to Fig. 1), this explains why the results of the calculations with different frequencies almost coincide at smaller fields. The figure also demonstrates the fact that the discrepancy between the IE model (dashed lines) and the full calculations (solid lines) increases with the intensity. Furthermore, the stabilizing effect turns out to be very weak in the fully correlated system. Whereas the full *ab initio* calculations give ionization probabilities that level off (low frequencies) or increase (high frequencies) for high intensities, the IE model returns probabilities that are noticeably lower. As the intensity grows, so does the discrepancy. As such, the simplified model tends to always underestimate the ionization probability, with the consequence that the stabilization effect is overestimated.

Note that for the highest frequencies considered in Figs. 1 and 3, the calculations extend into a region where the non-relativistic (dipole) approximation is likely to break down [15,30,31,52]. This is indicated in the figures. While we expect relativistic (nondipole) corrections to affect the calculated ionization probabilities to some extent in this region of field strengths, our analysis and conclusions are not dependent upon the affected subset of results and remain unaltered.

B. The role of electronic correlation

Figures 1 and 3 clearly demonstrate that the validity of the independent-electron model (11) breaks down in the superintense field regime. This may appear counterintuitive, as one might well expect the opposite to happen, i.e., that the importance of the electron-electron interaction should be negligible in the presence of a strong external perturbation. The reason why the electron-electron interaction in fact becomes

more important in this limit can be understood by analyzing the dynamics in the so-called Kramers-Henneberger (KH) frame [35–38], the rest frame of a classical free electron in the laser field. In this frame, the Hamiltonian, Eq. (1), is cast into the form

$$H_{\rm KH} = \sum_{i=1}^{2}\left(\frac{\mathbf{p}_i^2}{2} + V_{\rm KH}\left[\mathbf{r}_i + \boldsymbol{\alpha}(t)\right]\right) + \frac{1}{|\mathbf{r}_1 - \mathbf{r}_2|}, \tag{16}$$

where

$$V_{\rm KH}\left[\mathbf{r}_i + \boldsymbol{\alpha}(t)\right] = -\frac{2}{|\mathbf{r}_i + \boldsymbol{\alpha}(t)|} \tag{17}$$

is the Kramers-Henneberger potential, and

$$\boldsymbol{\alpha}(t) = \int_0^t A_z(t')\,dt'\hat{\mathbf{z}} \tag{18}$$

represents the position relative to the laboratory frame of a classical free electron in the electric field $E_z(t) = -\partial A_z/\partial t$. One characteristic feature of the KH frame is that the dipole interaction terms enter into the electron-nucleus Coulomb potentials [c.f. Eq. (17)], which in turn become time dependent and modified by the external field. Note also that the electron-electron interaction term is left unaffected by the HK transformation. Assuming for the moment that the Hamiltonian is periodic in time, i.e., neglecting the pulse profile, the KH potentials, Eq. (17), are expanded in a Fourier series as

$$V_{\rm KH}\left[\mathbf{r}_i + \boldsymbol{\alpha}(t)\right] = \sum_n V_n(\alpha_0, \mathbf{r}_i)e^{-in\omega t} \tag{19}$$

with

$$V_n(\alpha_0, \mathbf{r}_i) = \frac{1}{T}\int_0^T e^{-in\omega t} V_{\rm KH}\left[\mathbf{r}_i + \boldsymbol{\alpha}(t)\right]dt. \tag{20}$$

Inserting the expansion [Eq. (19)] into the TDSE and applying high-frequency Floquet theory, Gavrila *et al.* [10,53–55] showed that the $n = 0$ component in Eq. (20) plays an increasingly important role in the dynamics at higher values of α_0. Furthermore, in the limit of superintense fields ($\alpha_0 \gg 1$), Førre *et al.* [15] showed that the ionization dynamics of atomic hydrogen is mainly dictated by the V_0 potential. Thus, in this limit, the dynamics of the system is approximately given by the effective Hamiltonian

$$H_{\rm KH}^{\rm eff} = \sum_{i=1}^{2}\left(\frac{\mathbf{p}_i^2}{2} + V_0(\alpha_0, \mathbf{r}_i)\right) + \frac{1}{|\mathbf{r}_1 - \mathbf{r}_2|}. \tag{21}$$

Note that this Hamiltonian is time independent and accounts for *shake-up* (excitation) and *shake-off* (ionization) in the strong-field limit.

An analysis of the properties of the V_0 potential term in the vicinity of the origin reveals that it can be neglected relative to the electron-electron repulsion term in the limit $\alpha_0 \to \infty$, provided the two-electron wave function is localized, i.e., $\langle r_1\rangle \ll \alpha_0$ and $\langle r_2\rangle \ll \alpha_0$. This means that the dynamics of the two-electron system, in the limit of superintense fields and for sufficiently short pulses, ultimately reduces to that of a pure Coulomb explosion process effectuated by the Coulomb repulsion term in Eq. (21). From this, we conclude that the electron-electron interaction is in fact very important in the strong-field limit, effectively reducing the stabilization effect. Returning to the laboratory frame of reference, this should be understood in the following way: In the very-strong-field limit, the electrons effectively behave like free particles in the field, moving side by side with respect to the field axis. As this happens, the nuclear attraction may become less important than the mutual repulsion between the electrons, and the ionization is most likely initiated by electron-electron scattering events (Coulomb explosion) and not electron-nucleus collisions. This explains qualitatively why the ionization probabilities, calculated within the independent-electron model, deviate increasingly from the exact ones in the limit of stronger fields (cf. Figs. 1 and 3). As such, the observed deviation is indeed a manifestation of the breakdown of the single-particle picture in superstrong fields.

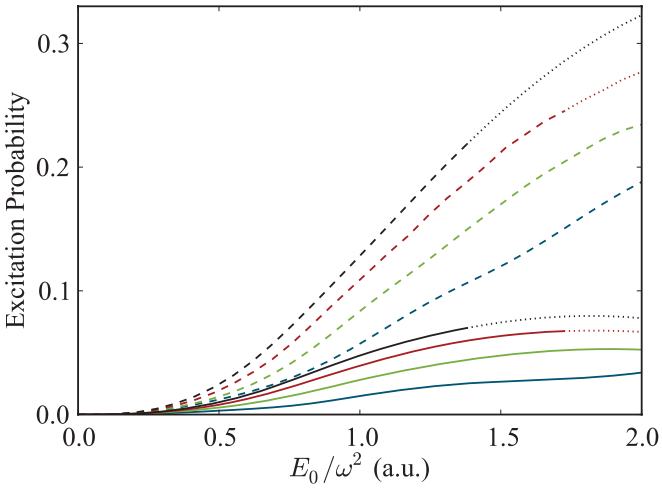

FIG. 4. (Color online) Excitation probabilities for the same scenario as in Fig. 3. The laser frequencies are $\omega = 10$, 8, 6, and 4 a.u. from top to bottom. The dashed lines are the results from the IE model, while the solid lines are the results from the full calculations. Relativistic (nondipole) effects may influence the results for high frequencies and field strengths (dotted curves).

Notice that the effective Hamiltonian in Eq. (21) only depends indirectly on the laser frequency through the displacement amplitude α_0, explaining why the validity of the IE model in Fig. 3 breaks down at approximately the same value of α_0 independent of the laser frequency.

Figure 4 shows the probability of excitation of helium for the cases considered in Fig. 3. Comparing Figs. 3 and 4, we observe that the decreasing ionization probability in the stabilization regime is accompanied by a corresponding increase in the excitation probability. Note that due to the high photon energy, excitation is here caused by shake-up processes, merely demonstrating the importance of the V_0 potential in the stabilization regime. The figure also clearly expresses the fact that shake-up is more important for the higher frequencies and that the IE model fails in describing shake-up (and shake-off) processes accurately, in accordance with the KH discussion above.

C. Analysis of angular and energy distributions

Further insight into the strong-field behavior of helium may be gained by examining the energy distribution of the ejected

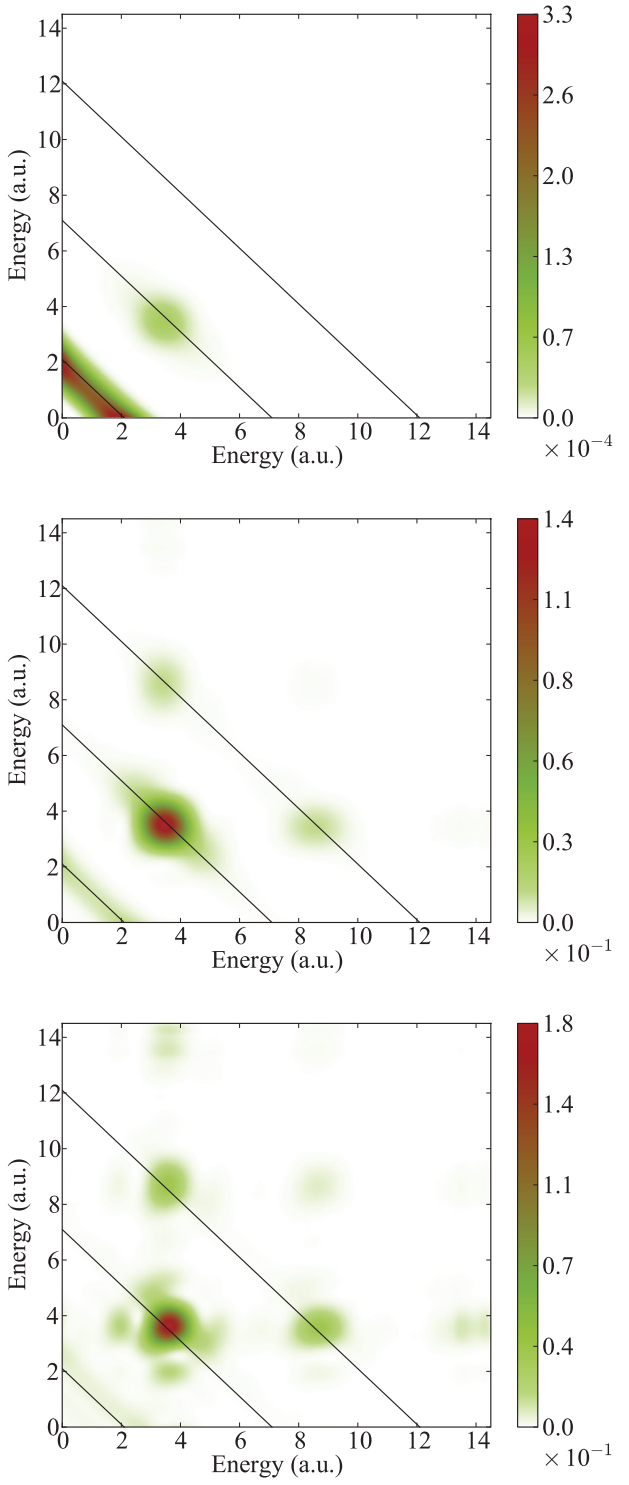

FIG. 5. (Color online) Double-ionization energy distribution for an $\omega = 5$ a.u. six-cycle pulse (182 as), and for field strengths of 1 (upper panel), 10 (middle panel), and 20 a.u. (lower panel).

electrons. In particular, imprints left by the electron interaction in the angular distribution of the outgoing electrons may give further clues as to its importance at the different field-strength regimes considered here.

In Fig. 5, the double-ionization energy distribution is shown for three different field strengths, 1, 10, and 20 a.u. (from top to bottom). The pulse duration was fixed at six cycles (182 as) with a frequency of 5 a.u. At the lower intensity (amplitude), one-photon ionization dominates as expected. As the intensity increases, two-photon ionization becomes prominent, and higher-order double-electron above threshold ionization (DATI) peaks start to appear [32]. Since the one-photon process is highly correlated and depends critically on the exchange of energy between the two electrons, it becomes less important at stronger fields, and two-photon double ionization takes over as the dominating channel. At the highest intensity, more structures appear in the energy spectrum, caused by sidebands in the pulse, and the one-photon-ionization process has become negligible.

The two-photon DATI component manifests itself as a single-peaked structure in Fig. 5, in contrast to the common double-peak structure associated with sequential ionization [32]. With the ultrashort pulse considered here, the second photon is absorbed before the residual ion has had time to relax to the ground state, but if the duration is increased to beyond 20 cycles, relaxation may occur and a double-peak structure appears (not shown here). The fact that the two peaks, corresponding to sequential two-photon double ionization in the long-pulse limit, shift toward each other in the short-pulse regime and eventually merge into one single peak (located at equal energy sharing) is well known and has been studied in a series of papers in the weak-field (perturbative) limit [33,56–65]. The results in Fig. 5 demonstrate that this feature survives in the superintense field regime, representing a clear departure from the independent-electron model [Eq. (11)].

Figure 6 shows the conditional angular distributions of the ejected electrons obtained at the two-photon DATI peak in Fig. 5, with equal energy sharing, and one of the electrons emitted along the polarization direction (indicated with an

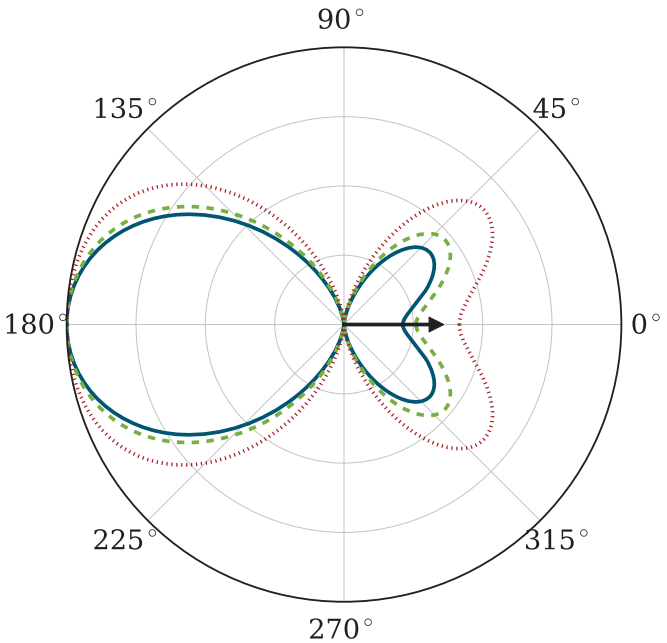

FIG. 6. (Color online) Angular distributions for double ionization with equal energy sharing $E_1 = E_2 = (2\omega - I_p)/2$. The arrow indicates the fixed direction of the first electron. Solid (blue) line: $E_0 = 1$ a.u. Dashed (green) line: $E_0 = 10$ a.u. Dotted (red) line: $E_0 = 20$ a.u.

arrow in the figure). The figure clearly shows that the distribution has a backward-forward asymmetry even at the highest intensity considered, demonstrating the breakdown of the single-particle picture, wherein a symmetric double-lobe (dipole) distribution would be found. The results are in accordance with recent results obtained at weaker fields [56,57,63], and shows that the back-to-back ejection mechanism is largely preserved even at very strong fields.

From numerical studies of stabilization in atomic hydrogen, it is known that the stabilization phenomenon is accompanied by the appearance of slow electrons [15]. As the intensity is increased beyond the ionization maximum, where stabilization sets in, and for sufficiently short pulses, a peak structure near zero energy appears in the electron energy spectrum, becoming increasingly dominant as the intensity becomes large. This may be understood from the Kramers-Henneberger analysis above and the importance of the V_0 potential in the limit of short, intense pulses. In order to provide a baseline comparison for the two-electron case considered here, we have calculated the

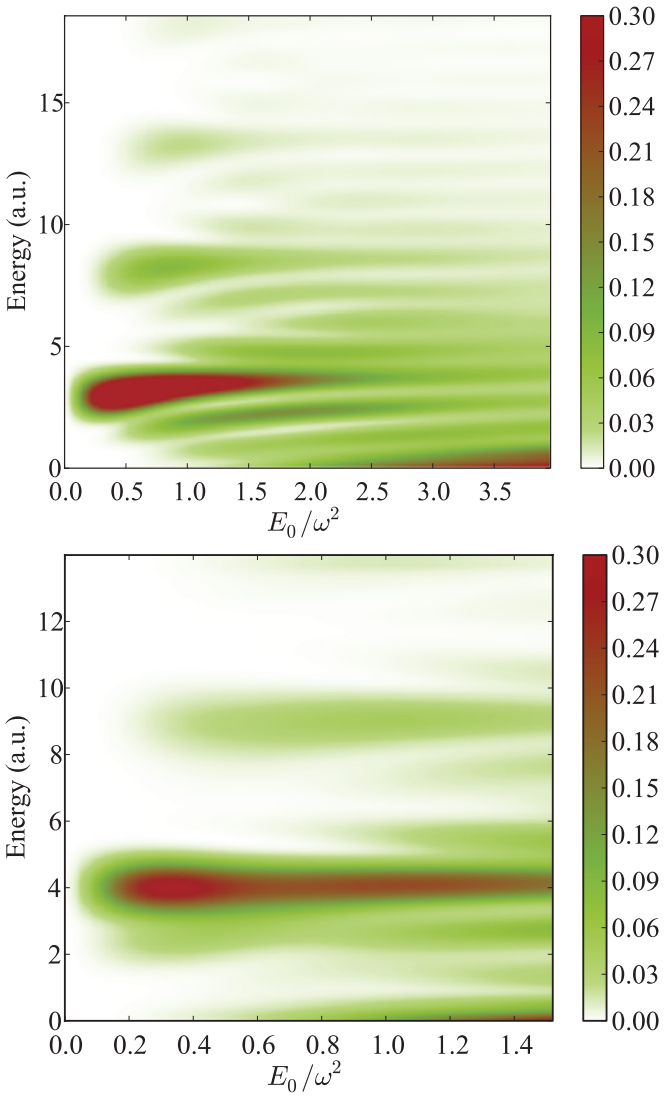

FIG. 7. (Color online) Energy distributions as a function of laser field strength. Top panel: He^+. Bottom panel: helium (single ionization). See text for details.

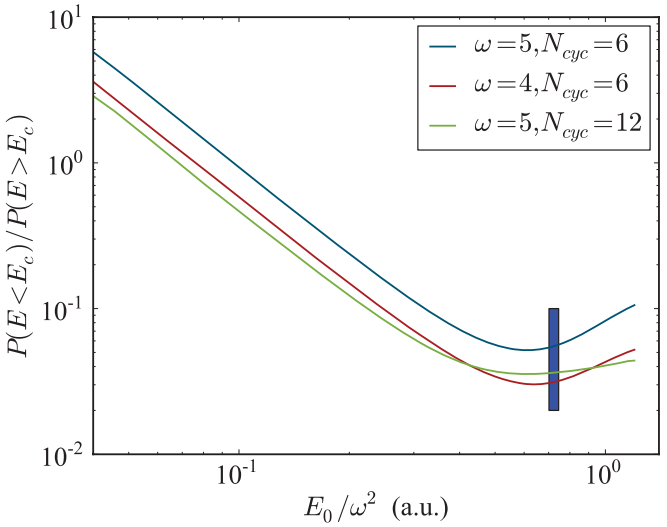

FIG. 8. (Color online) Ratio of slow to fast electrons for the double-ionization process, shown for different pulse frequencies and durations, and plotted as a function of α_0. The blue bar indicates the region where the corresponding double-ionization probability is maximum, where stabilization sets in.

energy distribution for ionization of He^+, with identical pulse characteristics as those used in Fig. 5. The result is shown in the upper panel of Fig. 7. We note the presence of above threshold ionization peaks, and, at the highest intensities, a slow electron peak (SEP) near zero energy [15,66]. The corresponding single-ionization energy distribution of helium is shown in the lower panel of Fig. 7, and indeed, a slow electron peak is visible. Note that the onset of slow electrons occurs at lower-field strengths in the single ionization of helium than in He^+, which is related to the different ionization potentials (I_p).

Now, examining the lower panel in Fig. 5, it appears that slow electrons do not emerge in the double-ionization process at this intensity. However, the ionization potential is greater than that for single ionization, and, therefore, higher intensities are needed to reach the regime where a SEP may appear. Since He^+, with an ionization potential of $I_p = 2$ a.u., exhibits an onset of slow electrons around 50 a.u., similar or possibly even higher-field strengths may be required for a SEP to appear in the double ionization of helium. We may, however, observe the onset of slow electrons by partitioning the double-ionization energy distribution into a low- and a high-energy part, and considering the ratio of these two (cf. Fig. 8). In this figure, values of the ratio $P(E < E_c)/P(E > E_c)$, where $E_c = 3/2\omega - I_p$, for different frequencies and pulse durations are shown, and in all cases, we observe an increase of low-energy electrons after the stabilization peak (indicated by the blue bar); however, it is most pronounced for the shorter pulses.

IV. CONCLUSION

In conclusion, we have presented an in-depth analysis of two-electron dynamics driven by high-intensity ultrashort laser pulses in the xuv regime. Expanding on our earlier investigation of correlation effects in the stabilization of helium, we

have shown that stabilization occurs within a narrow interval of values of α_0, independent of frequency and pulse duration. This is also the point at which an independent-electron picture begins to break down, demonstrating the important role of the electron-electron interaction at high intensities. Through an analysis of a high-intensity limit form of the Hamiltonian, expressed in the Kramers-Henneberger frame, this feature may be understood. Further indications of intense-field correlation effects are found in the angular distributions, where a backward-forward asymmetry is found for a wide range of intensities. Finally, we have shown that slow electrons emerge at high intensities, as they do in one-electron systems, but at different intensities for single and double ionization.

ACKNOWLEDGMENTS

This work was supported by the Bergen Research Foundation (Norway). The calculations were performed on the Cray XT4 (Hexagon) supercomputer at Parallab, University of Bergen (Norway). CPU hours were provided by NOTUR.

[1] M. Pont and M. Gavrila, Phys. Rev. Lett. **65**, 2362 (1990).
[2] Q. Su, J. H. Eberly, and J. Javanainen, Phys. Rev. Lett. **64**, 862 (1990).
[3] M. V. Fedorov and A. M. Movsesian, J. Phys. B **21**, L155 (1988).
[4] J. H. Eberly and K. C. Kulander, Science **262**, 1229 (1993).
[5] S. Geltman, J. Phys. B **27**, 257 (1994).
[6] M. Pont, N. R. Walet, M. Gavrila, and C. W. McCurdy, Phys. Rev. Lett. **61**, 939 (1988).
[7] K. C. Kulander, K. J. Schafer, and J. L. Krause, Phys. Rev. Lett. **66**, 2601 (1991).
[8] K. Burnett, P. L. Knight, B. R. M. Piraux, and V. C. Reed, Phys. Rev. Lett. **66**, 301 (1991).
[9] S. Geltman, Chem. Phys. Lett. **237**, 286 (1995).
[10] M. Gavrila, J. Phys. B **35**, R147 (2002).
[11] A. M. Popov, O. V. Tikhonova, and E. A. Volkova, J. Phys. B **36**, R125 (2003).
[12] K. Yamanouchi, S. L. Chin, P. Agostini, G. Ferrante, and M. Fedorov, in *Progress in Ultrafast Intense Laser Science I*, Springer Series in Chemical Physics, Vol. 84 (Springer, Berlin, 2006), pp. 1–18.
[13] R. Grobe and C. K. Law, Phys. Rev. A **44**, R4114 (1991).
[14] J. Grochmalicki, M. Lewenstein, and K. Rzkazewski, Phys. Rev. Lett. **66**, 1038 (1991).
[15] M. Førre, S. Selstø, J. P. Hansen, and L. B. Madsen, Phys. Rev. Lett. **95**, 043601 (2005).
[16] M. Dondera, H. G. Muller, and M. Gavrila, Phys. Rev. A **65**, 031405(R) (2002).
[17] R. Grobe and J. H. Eberly, Phys. Rev. A **47**, R1605 (1993).
[18] Q. Wei, S. Kais, and N. Moiseyev, Phys. Rev. A **76**, 013407 (2007).
[19] M. P. de Boer, J. H. Hoogenraad, R. B. Vrijen, L. D. Noordam, and H. G. Muller, Phys. Rev. Lett. **71**, 3263 (1993).
[20] N. J. van Druten, R. C. Constantinescu, J. M. Schins, H. Nieuwenhuize, and H. G. Muller, Phys. Rev. A **55**, 622 (1997).
[21] A. Talebpour, C.-Y. Chien, and S. L. Chin, J. Phys. B **29**, 5725 (1996).
[22] J. H. Hoogenraad, R. B. Vrijen, and L. D. Noordam, Phys. Rev. A **50**, 4133 (1994).
[23] T. Shintake *et al.*, Nature Photon. **2**, 555 (2008).
[24] W. Ackermann *et al.*, Nat. Photon. **1**, 336 (2007).
[25] E. Allaria, C. Callegari, D. Cocco, W. M. Fawley, M. Kiskinova, C. Masciovecchio, and F. Parmigiani, New J. Phys. **12**, 075002 (2010).
[26] M. Gavrila and J. Shertzer, Phys. Rev. A **53**, 3431 (1996).
[27] E. A. Volkova, V. V. Gridchin, A. M. Popov, and O. V. Tikhonova, JETP **99**, 320 (2004).
[28] A. M. Popov, O. V. Tikhonova, and E. A. Volkova, Laser Phys. **17**, 103 (2007).
[29] D. Bauer and F. Ceccherini, Phys. Rev. A **60**, 2301 (1999).
[30] A. Staudt and C. H. Keitel, J. Phys. B **36**, L203 (2003).
[31] A. Staudt and C. H. Keitel, Phys. Rev. A **73**, 043412 (2006).
[32] J. S. Parker, L. R. Moore, K. J. Meharg, D. Dundas, and K. T. Taylor, J. Phys. B **34**, L69 (2001).
[33] S. Laulan, H. Bachau, B. Piraux, J. Bauer, and G. L. Kamta, J. Mod. Opt. **50**, 353 (2003).
[34] T. Birkeland, R. Nepstad, and M. Førre, Phys. Rev. Lett. **104**, 163002 (2010).
[35] W. Pauli and M. Fierz, Nuovo Cimento **15**, 167 (1938).
[36] H. A. Kramers, *Collected Scientific Papers* (North-Holland, Amsterdam, 1956).
[37] W. C. Henneberger, Phys. Rev. Lett. **21**, 838 (1968).
[38] F. H. Faisal, J. Phys. B **6**, L89 (1973).
[39] H. G. Muller and M. Fedorov, *Super Intense Laser-Atom Physics*, Vol. 4 (Kluwer, Dordrecht, 1996).
[40] T. Birkeland and R. Nepstad, computer code PYPROP [http://pyprop.googlecode.com].
[41] C. de Boor, *A Practical Guide to Splines*, rev. ed. (Springer-Verlag, New York, 2001).
[42] H. Bachau, E. Cormier, P. Decleva, J. E. Hansen, and F. Martín, Rep. Prog. Phys. **64**, 1815 (2001).
[43] B. H. Bransden and C. J. Joachain, *Physics of Atoms and Molecules*, 2nd ed. (Pearson Education, Harlow, 2003).
[44] Y. Saad and M. H. Schultz, J. Sci. Stat. Comput. **7**, 856 (1986).
[45] Y. Saad, *Iterative Methods for Sparse Linear Systems* (SIAM, Philadelphia, 2003).
[46] J. Feist, S. Nagele, R. Pazourek, E. Persson, B. I. Schneider, L. A. Collins, and J. Burgdörfer, Phys. Rev. A **77**, 043420 (2008).
[47] L. B. Madsen, L. A. A. Nikolopoulos, T. K. Kjeldsen, and J. Fernández, Phys. Rev. A **76**, 063407 (2007).
[48] D. C. Sorensen, SIAM J. Matrix Anal. Appl. **13**, 357 (1992).
[49] R. Nepstad, T. Birkeland, and M. Førre, Phys. Rev. A **81**, 063402 (2010).
[50] S. Geltman, Phys. Rev. Lett. **54**, 1909 (1985).
[51] X. M. Tong and C. D. Lin, J. Phys. B **38**, 2593 (2005).
[52] S. Selstø, E. Lindroth, and J. Bengtsson, Phys. Rev. A **79**, 043418 (2009).
[53] M. Gavrila and J. Z. Kamiński, Phys. Rev. Lett. **52**, 613 (1984).
[54] M. Gavrila, *Atoms in Intense Laser Fields* (Academic, New York, 1992).
[55] M. Gavrila, I. Simbotin, and M. Stroe, Phys. Rev. A **78**, 033404 (2008).
[56] A. Palacios, T. N. Rescigno, and C. W. McCurdy, Phys. Rev. A **79**, 033402 (2009).

[57] J. Feist, S. Nagele, R. Pazourek, E. Persson, B. I. Schneider, L. A. Collins, and J. Burgdörfer, Phys. Rev. Lett. **103**, 063002 (2009).
[58] S. Laulan and H. Bachau, Phys. Rev. A **68**, 013409 (2003).
[59] K. L. Ishikawa and K. Midorikawa, Phys. Rev. A **72**, 013407 (2005).
[60] I. F. Barna, J. Wang, and J. Burgdörfer, Phys. Rev. A **73**, 023402 (2006).
[61] E. Foumouo, S. Laulan, B. Piraux, and H. Bachau, J. Phys. B **39**, S427 (2006).
[62] E. Foumouo, P. Antoine, H. Bachau, and B. Piraux, New J. Phys. **10**, 025017 (2008).
[63] A. Palacios, D. A. Horner, T. N. Rescigno, and C. W. McCurdy, J. Phys. B **43**, 194003 (2010).
[64] E. Foumouo, A. Hamido, P. Antoine, B. Piraux, H. Bachau, and R. Shakeshaft, J. Phys. B **43**, 091001 (2010).
[65] T.-G. Lee, M. S. Pindzola, and F. Robicheaux, Phys. Rev. A **79**, 053420 (2009).
[66] K. Toyota, O. I. Tolstikhin, T. Morishita, and S. Watanabe, Phys. Rev. Lett. **103**, 153003 (2009).